Chemical Physics Letters 582 (2013) 115–118

Contents lists available at ScienceDirect

Chemical Physics Letters

journal homepage: www.elsevier.com/locate/cplett

Characterization of graphene–fullerene interactions: Insights from density functional theory

S. Laref [a], A.M. Asaduzzaman [a], W. Beck [b], P.A. Deymier [a], K. Runge [a], L. Adamowicz [c], K. Muralidharan [a,*]

[a] Department of Materials Science and Engineering, University of Arizona, Tucson, AZ 85721, USA
[b] Department of Physics, University of Arizona, Tucson, AZ 85721, USA
[c] Department of Chemistry and Biochemistry, University of Arizona, Tucson, AZ 85721, USA

ARTICLE INFO

Article history:
Received 10 June 2013
In final form 17 July 2013
Available online 23 July 2013

ABSTRACT

Using density functional theory (DFT) based approaches that utilize appropriate semi-empirical and non-local van der Waals corrections, we rigorously examine the interactions between fullerene (C_{60}) molecules and pristine single layer graphene (SLG) sheets as well as SLG containing isolated mono-vacancy, divacancy and Stone–Wales defect-sites respectively. Our results show that chemical bonding between the C_{60} molecule and SLG at mono-vacancy defect-sites demonstrate predominantly sp^3-like hybridization, in contrast to weaker π–π interactions that characterize C_{60}–SLG systems containing divacancies and Stone–Wales defects.

1. Introduction

The remarkable structure property relations exhibited by low-dimensional carbon nanostructures such as single-sheet graphene (SLG), fullerenes (C_{60}) and carbon nanotubes (CNT), has spurred a growing interest in fabricating corresponding hybrid nanostructures for a wide range of applications including electronics, spintronics, energy harvesting, and energy storage applications. Theory-based and experimental investigations have demonstrated the feasibility of SLG–CNT based hybrid structures [1,2], while robust CNT–C_{60} structures are yet to be realized. Since pristine SLG is known to interact with C_{60} via weak van der Waals (vdW) forces, methods that promote strong chemical bonding between C_{60} and SLG need to be explored in order to pave way for fabricating hybrid C_{60}–SLG nanostructures. Two possible routes for facilitating strong C_{60}–SLG interactions include (i) chemical functionalization of SLG and/or C_{60} leading to chemical-bond formation and (ii) defect-mediated chemistry, where the higher reactivity of the defect sites induce chemisorption of C_{60} on SLG. While Yu et al. [3] have already examined the usage of chemical functionalization groups to ensure chemical attachment of C_{60} on SLG, there is not much available information on quantifying the role of defects in enabling strong chemical interactions between SLG and C_{60} molecules. Towards this end, as an important first step, using density functional theory (DFT) we examine energy-minimized C_{60}–SLG hybrid-structures, and quantify the effect of various intrinsic SLG defects (mono-vacancy, di-vacancies and Stone–Wales defect) that are stable at room temperature [28], on the binding energetics and geometries of the hybrid structures.

DFT has become the electronic-structure method of choice for providing a first-principles understanding of molecular-adsorption mechanisms on surfaces and extended systems [4–6]. Nevertheless, the popular descriptions for the exchange–correlation functionals in DFT, namely local density approximation (LDA) and the generalized gradient approximation (GGA) do not define weak noncovalent dispersive vdW interactions with sufficient precision and hence corrections to the energy functionals are required to account for these shortcomings, especially for graphitic systems, as discussed by Dappe et al. [7].

Building on the work of Dappe et al. [7], in the present study, we employ GGA functionals with semi-empirical and non-local vdW corrections, within the framework of computationally efficient plane-wave DFT, to model the interactions between C_{60} and pristine and defected SLG sheets. A hierarchy of intrinsic defects within SLG is considered namely mono-vacancy, Stone–Wales, pentagon–octagon–pentagon (5–8–5) divacancy, and a tri-pentagon–tri-heptagon (555–777) reconstructed divacancy [8–13]. For each C_{60}–SLG hybrid-nanostructure, the binding energetics, the corresponding minimum-energy configuration as well as changes in electronic-structure that underlie the nature of binding are characterized.

2. Methodology

The DFT calculations were carried out using the Vienna *ab initio* Simulation Package VASP.5.2 [14]. The projected augmented wave formalism (PAW) was employed to model the electron–ion interactions [15]. The exchange–correlation functionals followed the standard generalized gradient approximation of Perdew–

* Corresponding author. Fax: +1 520 626 8059.
E-mail address: Krishna@email.arizona.edu (K. Muralidharan).

0009-2614/$ - see front matter © 2013 Elsevier B.V. All rights reserved.
http://dx.doi.org/10.1016/j.cplett.2013.07.033

Burke–Ernzerhof (GGA–PBE) [16], and in addition, two modified PBE functionals incorporating different flavors of vdW corrections were also utilized. Specifically, the (i) vdW semi-empirical PBE-D2 correction as established by Grimme [17–18], and the (ii) non-local method of Klimeš et al. (optB86b) [19] were employed in our studies.

The two dimensional single layer graphene (SLG) sheets were represented by an 8×8 periodic supercell consisting of 128 atoms; the different defects were created at the center of the supercell. A vacuum region of 24 Å was introduced perpendicular to the SLG sheet to prevent unphysical periodic effects. This strategy was also employed for the case of examining C_{60} adsorption on SLG.

Given the large size of the supercell, the numerical integration was carried out over the Brillouin zone using a $1 \times 1 \times 1$ Monkhorst–Pack k-point grid [20]. The pseudo-wave functions were expanded in a plane-wave basis set with an energy cut-off of 400 eV, and accuracy was ensured by adopting an energy-convergence criteria of 10^{-5} eV. Simultaneously, structural relaxation was carried out using the conjugate gradient technique, until the force on each atom was below 0.02 eV/Å.

The binding energy (E_{Bind}) of the various C_{60}–SLG systems was estimated by evaluating the energy of the structurally optimized (i) C_{60}–SLG system (E_{Tot}), SLG with and without defects (E_{Gr}), and an isolated C_{60} molecule (E_{C60}). In each case, $E_{Bind} = -(E_{Tot} - E_{Gr} - E_{C60})$.

3. Results and discussion

3.1. C_{60}–pristine SLG interactions

Four energetically favorable physisorption geometries of C_{60} on pristine SLG were identified as shown in Figure 1. Specifically, they are denoted as (i) BRI: where a C–C dimer shared by neighboring hexagons in the C_{60} molecule is aligned with a C–C bond in SLG, leading to an alignment of two hexagonal rings within the SLG and C_{60} respectively; (ii) C-RING: a C_{60} hexagon ring is aligned with another hexagon ring in SLG; (iii) C-ATP: a single carbon atom of the C_{60} molecule is directly atop a carbon atom of SLG; (iv) C-RING2: the center of a hexagon ring of C_{60} is aligned with a carbon atom of SLG.

Table 1 lists the corresponding binding energies as evaluated using PBE, PBE-D2 and optB86 for the identified adsorption geometries. Interestingly, all methods predict the C-ATP geometry to be the most stable (i.e. the highest binding energy). Further, all methods predict similar variations in binding energies for the different geometries. PBE severely underestimates the binding energies due to the lack of dispersion corrections, while the vdW-incorporated methods predict the binding energy to be of the order of 1 eV, consistent with the observation of Dappe et al. [7]. Further, for a given adsorption geometry, optB86 predicts higher binding energies relative to PBE-D2. This can be attributed to the method of implementation of the adopted vdW approximations; specifically, for the case of the semi-empirical corrections, neither repulsion that arises from the overlap of electronic densities nor multipole effects are accounted for. For the non-local method, the corrections to the long-range correlations are incomplete due to restrictions imposed by using double-space integrals to express the non-local correlation energy [21].

The choice of including dispersion effects also affects the predicted equilibrium C_{60} adsorption distances (see Table 2). PBE consistently overestimates the adsorption distance with respect to vdW-incorporated methods; when vdW corrections are included, however, the predicted adsorption distance for the C-ATP configuration (i.e. the most stable geometry) is in good agreement with the previously reported theoretical and experimental results [7,22–24]. For the BRI and Ring geometries, the relatively larger adsorption distance, can be correlated to the zone facets symmetry between the C_{60} molecule and graphene surface [24]. A more detailed analysis relating the interplay between the choice of the vdW correction and the binding energy characteristics will be presented in a follow-up Letter.

It should be noted that energetically favorable adsorption geometries have also been identified by Švec et al., who used localized-orbitals (LCAO–S^2 + vdW) based DFT calculations to characterize C_{60}–SLG interactions [24]. A notable difference between the two studies is the fact that the size of the supercell is much larger in our Letter, hence we restrict our investigations to

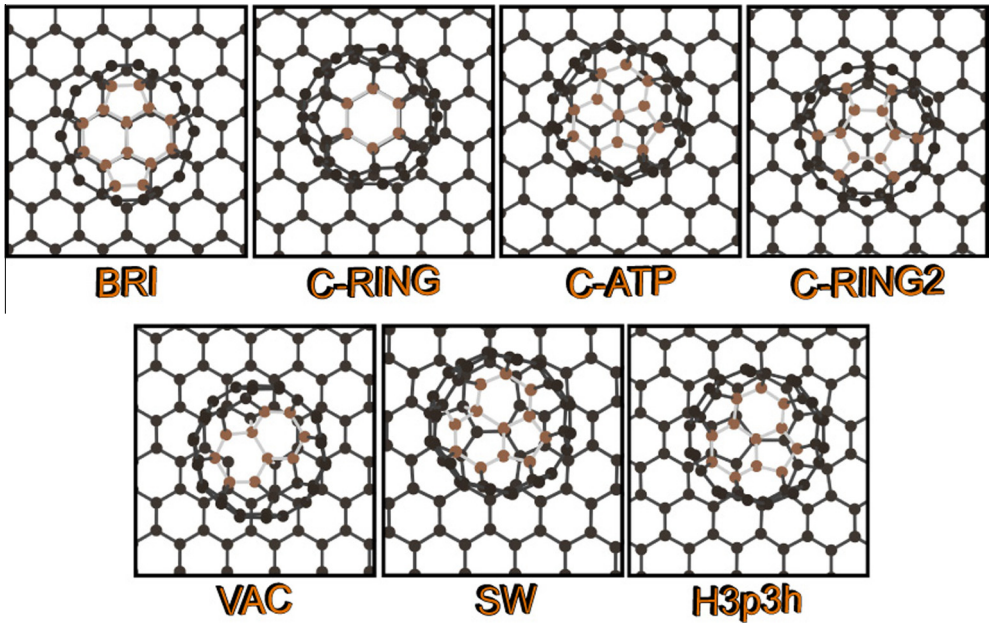

Figure 1. The adsorption geometries of C_{60} on pristine (top) and defected (below) SLG. The C_{60} atoms close to the SLG surface are brown in color, for ease of viewing. (For interpretation of the references to color in this figure legend, the reader is referred to the web version of this article.)

Table 1
The C_{60}–SLG binding energy (in eV) for the various geometries identified in this work, as evaluated by the three different methods. For comparison, available literature data (both theory-based and experimental estimations) are provided below.

Adsorption	PBE	PBE-D2	optB86b
BRI	0.13	0.84	1.20
C-RING	0.13	0.83	1.17
C-ATP	0.15	0.91	1.28
C-RING2	0.13	0.90	1.23
VAC	1.45	2.91	3.19
dVAC	0.09	0.82	1.14
SW	0.10	0.48	1.05
H3p3h	0.09	0.82	1.13

E_{Bind}(Exp.) = 0.85 eV (Ref. [22]).
E_{Bind}(Theo.) = 1 eV (Refs. [5,24]).

Table 2
The C_{60} adsorption distance (in Å) corresponding to the different geometries identified in this work, as evaluated by the three different methods. For comparison, available literature data (both theory-based and experimental estimations) are provided below.

Adsorption	PBE	PBE-D2	optB86b
BRI	3.57	3.10	3.14
C-RING	3.79	3.32	3.35
C-ATP	3.50	2.82	2.81
C-RING2	3.53	3.15	3.16
VAC	1.56	1.55	1.55
dVAC	3.54	2.93	2.90
SW	4.11	4.08	3.40
H3p3h	3.52	2.83	2.83

C–C distance (Theo.) = 2.9 Å (Ref. [7]).
C–C distance (Exp.) = 2.9 Å (Ref. [22]).

SLG-isolated C_{60} molecule interactions. Further, we allow for unrestricted geometry-optimization to identify the energy-minimized adsorbed structures in our studies.

3.2. C_{60}–defected SLG interactions

SLG sheets containing (i) a mono-vacancy (VAC), (ii) a 5–8–5 divacancy (dVAC), (iii) the Stone–Wales defect (SW), and (iv) a 555–777 reconstructed divacancy (H3p3h) were geometrically optimized. The corresponding defect-formation energies (E_f) are given in Table 3, and the predicted trends agree well with literature-data [25–29]. Nevertheless, it is worth noting that the predicted E_f value for the 5–8–5 divacancy is lower than that reported in Ref. [30], a consequence of the fact that Ref [30] examines hydrogen terminated graphene clusters within the LDA–DFT framework that utilize a Gaussian basis.

The geometrically optimized defected SLG systems were probed by a C_{60} molecule, and the most-stable geometries of the different defected SLG–C_{60} systems are shown in Figure 1. An important distinguishing feature characterizing the interaction of VAC with C_{60} is the large binding energy (see Table 1) indicating strong chemisorption of C_{60} on SLG containing a single vacancy. This is also reflected by the corresponding adsorption distance of 1.55/1.56 Å (depending on the method used) as given in Table 2. PBE underestimates the binding energy, while the predicted adsorption distances are consistent with PBE-D2 and optB86b results, pointing out the need for vdW corrections, despite the fact that PBE is able to accurately represent bond-formation between VAC and C_{60}. For the other defected systems, the most stable geometries as predicted by all methods correspond to physisorbed orientations of C_{60} as evident from the binding energies (see Table 1) and corresponding adsorption distances (see Table 2). Also, while we do observe energetically stable chemisorption of C_{60} on dVAC systems, the physisorbed geometry is energetically more favorable by around 0.1 eV and hence we do not consider the chemisorbed dVAC systems further in our discussion. Further, based on the energetics, it can be inferred that the SW–C_{60} system is the least stable, as also seen by the corresponding larger adsorption distance. Interestingly, the trends in the binding energies of the different C_{60}-defected-SLG systems correlate well with the observed trends in the respective defect-formation energies, represented in Table 3.

Table 3
Defect formation energies (E_f) for the various intrinsic point defects studied in this work as evaluated by the three different methods. For comparison, available literature data are provided below.

Adsorption	Other works	PBE	PBE-D2	optB86b
VAC	7.90 [25], 7.78 [26], 7.60 [27]	7.61	7.65	7.56
dVAC	7.60 [29], 8.5 [30]	7.33	7.34	7.36
SW	3.80 [25], 4.75 [26], 4.80 [27]	4.54	4.66	4.56
H3p3h		6.58	6.59	6.64

These observations can be analyzed based on the defect-site geometry. The VAC system is characterized by significant reconstruction around the mono-vacancy, with the local-structure consists of a nine-membered ring that contains an under-coordinated carbon atom (C_1), and an adjoining pentagon ring that shares a common high-strain C–C bond (C_2 and C_3) with the nine-membered ring (see Figure 2). This C–C bond-distance equals 2.02 Å as compared to the equilibrium 1.42 Å, and together with the under-coordinated C_1 atom, they represent chemically reactive sites. Consequently, the chemisorption of C_{60} is characterized by the formation of two chemical bonds between C_{60} and SLG, with a pair of adjacent carbon atoms of the C_{60} forming respective covalent bonds with C_1 and either of C_2 or C_3. In this process, the C_2–C_3 bond is further weakened and extends to 2.54 Å. In contrast, the other defected-SLG structures reconstruct to ensure the absence of dangling bonds, which impedes C_{60} chemisorption.

Supporting electron density plots reveal the formation of directional covalent bonds between the C_{60} and VAC–SLG as seen in Figure 3. Specifically, Figure 3a illustrates the spatial 3-D electronic charge difference profile ($\Delta\rho(r)$) of VAC–SLG, where r is a spatial coordinate. $\Delta\rho(r)$ is defined in terms of the electron density of the VAC–SLG system ($\rho_{C60-SLG}(r)$), the corresponding isolated C_{60}

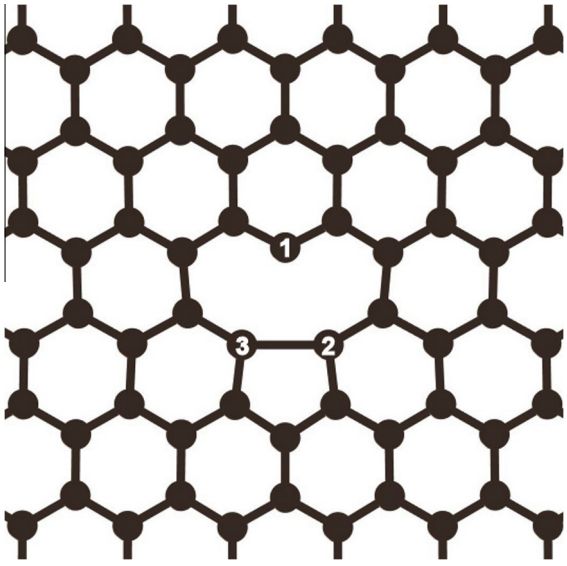

Figure 2. Minimum energy configuration of SLG containing an isolated monovacancy.

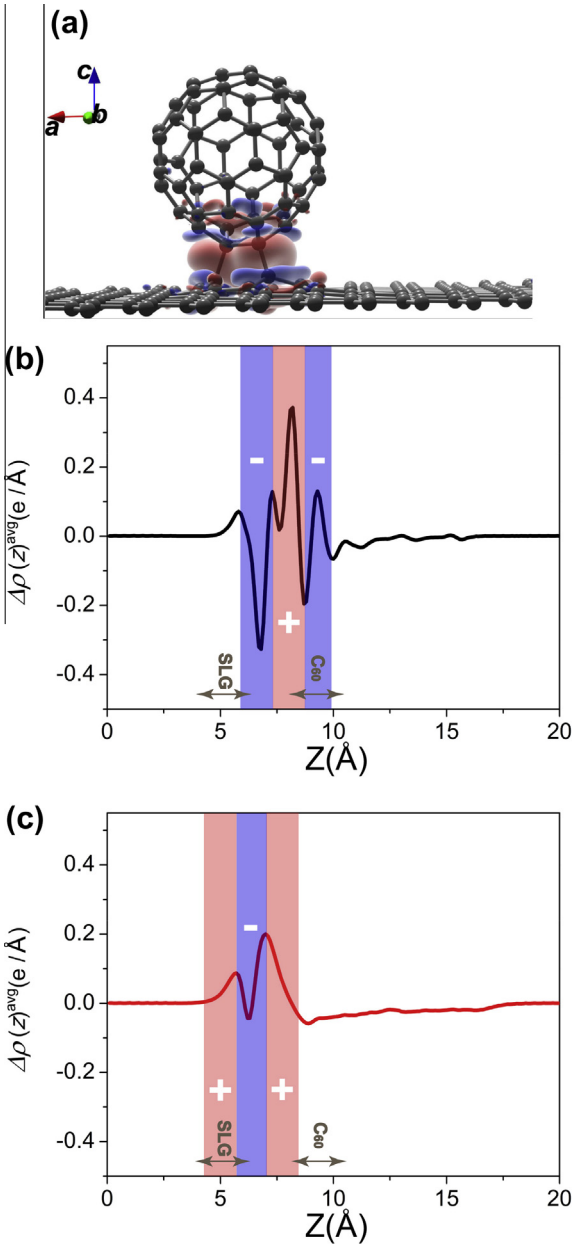

Figure 3. (a) 3-D view of the electronic charge density difference $\Delta\rho$ for the C_{60}-VAC system as obtained from the PBE-D2 method. The red and blue colors indicate electron accumulation and depletion respectively. Corresponding 1-D averaged electron-density difference ($\Delta\rho(z)$) along the adsorption direction for (b) VAC and (c) C-ATP respectively (the arrow indicate graphene and C60 positions with respect to *Z* axes).

$(\rho^{iso}_{C60}(r))$ and the defected-SLG $(\rho^{iso}_{SLG}(r))$ as follows: $\Delta\rho(r) = \rho_{C60-SLG}(r) - \rho^{iso}_{C60}(r) - \rho^{iso}_{SLG}(r)$. Additionally, Figure 3b illustrates a 1-D averaged electronic charge difference as a function of distance along the direction of adsorption. From these figures, it is clear that regions of electron accumulation (red lobes in Figure 3a and a + sign in Figure 3b) and electron depletion (blue lobes in Figure 3a and a − sign in Figure 3b) at the C_{60} and SLG boundaries are observed, unequivocally indicating the chemical attachment of C_{60} on VAC–SLG. In contrast, the physisorbed systems are characterized by electron-localization at the C_{60} and SLG boundaries respectively and do not exhibit covalent bond-formation as seen in Figure 3c, which depicts the 1-D averaged electron–density difference plots for the C-ATP system.

4. Conclusions

By explicitly including vdW corrections within the DFT framework, interactions between an isolated C_{60} molecule and pristine and defected SLG were accurately characterized. Energetically stable adsorption geometries of C_{60} on pristine SLG were examined and identified to be typical of physisorption. Further, C_{60} interactions with SLG containing different intrinsic point-defects were studied. SLG containing an isolated mono-vacancy chemically bonded with the C_{60} molecule via the formation of two covalent C–C bonds. In contrast, C_{60} physisorbed on SLG containing either isolated Stone–Wales defects or divacancies. The chemisorption of C_{60} in the presence of a mono-vacancy was attributed to the presence of an undercoordinated carbon atom at the defect-site. These observations, while not unexpected, have profound implications for the fabrication of hybrid C_{60}–SLG nanostructures; specifically, appropriate defect-engineering could enable the formation of robust, thermally and mechanically stable C_{60}–SLG lattices with interesting structure–property relations.

Acknowledgement

This work was supported by the National Science Foundation under Grant 1148936.

References

[1] F. Du, D. Yu, L. Dai, S. Ganguli, V. Varshney, A. Roy, Chem. Matter. 23 (2011) 4810.
[2] G. Dimitrakakis, E. Tylianakis, G. Froudakis, Nano Lett. 8 (2008) 3166.
[3] D. Yu, K. Park, M. Durstock, L. Dai, J. Phys. Chem. Lett. 2 (2011) 1113.
[4] J. Zhao, J.W. Jiang, Y. Jia, W. Guo, T. Rabczuk, Carbon 57 (2013) 108.
[5] L.M. Liu, M. Krack, A. Michaelides, J. Am. Chem. Soc. 130 (2008) 8572.
[6] S. Laref, L. Yan, M.-L. Bocquet, F. Delbecq, P. Sautet, D. Loffreda, Phys. Chem. Chem. Phys. 13 (2011) 11827.
[7] Y.J. Dappe, J. Ortega, F. Flores, Phys. Rev. B 79 (2009) 165409.
[8] M.M. Ugeda, Phys. Rev. B 85 (2012) 121402.
[9] A. Hashimoto, K. Suenaga, A. Gloter, K. Urita, S. Iijima, Nature 430 (2004) 870.
[10] J.C. Meyer, C.O. Girit, M.F. Crommie, A. Zettl, Nature 454 (2008) 319.
[11] M.H. Gass, U. Bangert, A.L. Bleloch, P. Wang, R.R. Nair, A.K. Geim, Nat. Nanotechnol. 3 (2008) 676.
[12] M.M. Ugeda, I. Brihuega, F. Guinea, J.M. Gómez-Rodríguez, Phys. Rev. Lett. 104 (2010) 096804.
[13] J. Coraux, A.T. N'Diaye, C. Busse, T. Michely, Nano Lett. 8 (2008) 565.
[14] G. Kresse, J. Furthmüller, Comput. Mater. Sci. 6 (1996) 15 (Phys. Rev. B 54 (1996) 11169).
[15] G. Kresse, D. Joubert, Phys. Rev. B 59 (1999) 1758.
[16] J.P. Perdew, K. Burke, M. Ernzerhof, Phys. Rev. Lett. 77 (1996) 3865.
[17] S. Grimme, J. Comput. Chem. 25 (2004) 1463.
[18] S. Grimme, J. Comput. Chem. 27 (2006) 1787.
[19] J. Klimeš, D.R. Bowler, A. Michaelides, Phys. Rev. B 83 (2011) 195131 (J. Phys.: Condens. Matter. 22 (2010) 022201).
[20] H.J. Monkhorst, J.D. Pack, Phys. Rev. B 13 (1976) 5188.
[21] N. Marom, J. Chem. Theory Comput. 7 (2011) 3944.
[22] H. Ulbricht, G. Moos, T. Hertel, Phys. Rev. Lett. 90 (2003) 095501.
[23] D. Feller, K.D. Jordan, J. Phys. Chem. A 104 (2000) 9971.
[24] M. Švec, Phys. Rev. B 86 (2012) 121407.
[25] B. Wang, Y. Puzyrev, S.T. Pantelides, Carbon 49 (2011) 3983.
[26] Z. Wang, Y.G. Zhou, J. Bang, M.P. Prange, S.B. Zhang, G. Fei, J. Phys. Chem. C 116 (2012) 16070.
[27] L. Li, S. Reich, J. Robertson, Phys. Rev. B 72 (2005) 184109.
[28] F. Banhart, J. Kotakoski, A.V. Krasheninnikov, ACS Nano 5 (2011) 26.
[29] D.J. Appelhans, L.D. Carr, M.T. Lusk, New J. Phys. 12 (2010) 125006.
[30] A.A. El-Barbary, R.H. Telling, C.P. Ewels, M.I. Heggie, P.R. Briddon, Phys. Rev. B 68 (2003) 144107.